Experimental Mechanics (2010) 50:845–865
DOI 10.1007/s11340-010-9381-z

Experimental Fracture Mechanics of Functionally Graded Materials: An Overview of Optical Investigations

C.-E. Rousseau · V.B. Chalivendra · H.V. Tippur · A. Shukla

Received: 30 March 2010 / Accepted: 7 June 2010 / Published online: 15 July 2010

Abstract The experimental efforts towards understanding the fracture behavior of continuously graded Functionally Graded Materials (FGMs) using full-field optical methods are reviewed. Both quasi-static and dynamic fracture investigations involving mode-I and -II conditions are presented. FGM configurations with crack planes perpendicular to, parallel to, and inclined to the direction of compositional gradation are discussed. Different strategies adopted by various investigators to develop polymer-based FGM systems for experimental mechanics studies are also described in this overview. Major theoretical developments that have predated and paralleled the experimental studies have been presented as well. Finally, the paper notes a few potential new directions where further contributions are possible.

This is the 5th in a series of featured review articles to celebrate the 50th anniversary of Experimental Mechanics. These articles serve to touch on both areas of mechanics where the journal has contributed extensively in the past and emergent areas for the future.

C.-E. Rousseau · A. Shukla (SEM Fellow)
University of Rhode Island, Kingston, RI, USA

C.-E. Rousseau
e-mail: rousseau@uri.edu

A. Shukla
e-mail: shuklaa@egr.uri.edu

V.B. Chalivendra (SEM member)
University of Massachusetts, Dartmouth, MA, USA
e-mail: vchalivendra@umassd.edu

H.V. Tippur (✉, SEM member)
Auburn University, Auburn, AL, USA
e-mail: htippur@eng.auburn.edu

Keywords Functionally graded materials · CGS · Photoelasticity · DIC · Fracture Mechanics

Introduction

The concept of Functionally Graded Materials (FGMs) arose from the early attempts to meet stringent material requirements pertaining to aerospace vehicles facing thermal cycles between elevated and cryogenic temperatures. The demands of achieving adequate toughness, resilience, compliance, and rigidity goals simultaneously motivated the early investigations. This goal is most efficiently met by assembling different materials with those desirable properties, while ensuring seamless and smooth spatial variation from one material to the other, thereby circumventing the deleterious effects such as residual stresses, planes of weakness, or stress concentration present in case of discrete interfaces. The gradual variation in material properties in the resulting composite has been indeed shown to improve failure performance, while preserving the intended thermal, tribological, and structural benefits of combining dissimilar materials [1]. Practical examples of such designs include the gradual amalgamation of tungsten and zirconia in ratios of 80:20, 60:40, 40:60, and 20:80, respectively. Other systems include titanium–titanium boride, titanium–zirconia, tungsten–silicon, and other metal–ceramic combinations. A gradual variation of porosity by the infusion of voids is also considered for lightweight structural applications. The concept, however innovative as it may appear, can be abundantly seen in nature. Some common examples include cross-sectional microstructures found in bamboo shafts and animal bones. Although most works on FGMs to date

focus on thermal properties and elastic wave channeling, their ability to resist fracture is also of significant interest. Therefore, the aim of this paper is to review the state-of-the-art in this specific area of experimental fracture mechanics aided by full-field optical methods. The approach taken here is one wherein material variation in elastic modulus plays the principal role is influencing fracture properties. It is implicit, however, that other factors such as variations in fracture toughness will also play a role in guiding the behavior of the crack. For instance, Jin and Batra [2] expounded on a theory where they ascribed prominence to that parameter. Other factors such as density would also affect FGM fracture, especially during crack propagation. Nevertheless, most studies tend to emphasize Young's modulus variations, as done throughout this manuscript.

A variety of processing methods have emerged over the years for preparing FGMs. For instance, Sasaki and Hirai [3] have fabricated FGMs using chemical vapor deposition. Bishop et al. [4] employed powder metallurgy. Chu et al. [5] made use of slip casting technique, whereas Sampath et al. [6] utilized plasma spraying. These methods largely influence the microstructure and hence macro-mechanical responses of FGMs. An additional differentiation regarding stepwise (or discrete) [7] versus continuous compositional variations [8] can also be made. The former category encompasses homogeneous materials that are layered in a stepwise fashion until the desired profile is attained whereas in the latter the same is achieved by a continuous variation of composition on a macroscale. Parameswaran and Shukla [9] also developed continuous graded materials using a gravity assisted casting process and characterized these FGMs for Young's modulus and fracture toughness. In this work, *the discussion is limited to the response of those with continuous variation of properties*. It should be emphasized that continuity in the context of FGMs is used in the macroscopic sense. Indeed, most optical techniques are not capable of performing below the millimeter scale, whereas the particulate composites used here, have representative volume elements limited to the tens of micrometer range. Therefore, the continuity assumption relates solely to the overall gradation profile of the material.

It is further noted that despite the several fabrication techniques and proposed FGM systems, as listed above, researchers have not performed specific experiments involving these *real* materials. Instead, the focus has been on *model* materials fabricated in small quantities. These model materials involved irradiated plastics, thermosets, polymeric materials, sometimes interspersed with particulates. Compared to real materials, they are far more cost effective, yet also hold the promise of implementation within real structures.

Theoretical interest in the fracture mechanics of nonhomogeneous materials predates its recent revival in the context of functionally graded materials. These include, for instance, the contributions of Atkinson and List [10] and Delale and Erdogan [11]. Several refinements to the theory and the proposed solutions have succeeded for nearly two decades, unaided by experimentation. The latter was impeded generally by the complexities associated with preparation of such materials in a consistent and controlled fashion. Recent advances in this regard have naturally let significant experimental mechanics studies to emerge. Amongst those, *fracture experiments performed on FGMs will be limited to those conducted by means of optical tools are reviewed in this overview*.

This paper will first proceed with an evolutionary account of the theory of fracture of nonhomogeneous materials essential for interpreting optically measured crack tip fields. Optical investigations performed respectively, with cracks perpendicular, and cracks parallel to the gradient directions are then addressed. This is followed by a description of dynamic experiments, solely for cracks parallel to the gradient direction but resulting in pure mode-I and mixed-mode behaviors. Throughout the paper, several materials and optical systems are described chronologically as applied to FGM research. Finally, the paper concludes with a section listing several areas where new experimental research could lead to a better understanding of the fracture behavior in FGMs, and a summary of contributions to the field.

Crack-Tip Stress Fields

Much of the experimental work towards understanding the behavior of graded materials weakened by cracks has risen from the need to first verify the theoretical formulations guiding the field. A common aspect of this theoretical cluster, dating from the 1970's, uses an exponential variation of elastic properties. That is, the shear modulus is often expressed as:

$$\mu(x, y) = \mu_0 e^{(\beta x + \gamma y)}, \tag{1}$$

where β and γ define the spatial variations of the material along the x- and y- directions, respectively. This specific formulation, featuring an exponential gradation, is by far the most common, owing to the relative ease of manipulation of the compatibility equation. Other situations involving, for instance, linear variations would present a far more daunting task. The

coordinates x and y are universally described as being aligned in directions parallel to and normal to the crack face, respectively, with the crack tip as the origin (see Fig. 1). In situations where material inertia is important as in dynamic crack growth cases, the mass density is made to follow an identical variation. (It should be noted that the variations in Poisson's ratio have been found less important (e.g., Delale and Erdogan [11]).

The above mentioned researchers have offered one of the earliest solutions for a crack embedded within a nonhomogeneous planar solid subjected to arbitrary, quasi-static, boundary tractions using the method of integral equations. It revealed the standard square root stress singularity at the crack tip as in the homogeneous counterparts. Specific equations were established for obtaining stress intensity factor for the case of a uniformly pressurized crack. Differences between plane stress and plane strain assumptions were found to be minimal. Experimental validation of this specific solution is difficult and is yet to be attempted.

Using Williams' eigenfunction expansion technique [12], Eischen [13] derived the quasi-static stress and in-plane displacement fields, (u_x, u_y), for the case of a nonhomogeneous material with elastic properties described by a Maclaurin series expansion. The first few terms of displacement expressions are as follows:

$$\begin{aligned} u_x = {} & \frac{K_I}{\mu_0}\sqrt{\frac{r}{2\pi}}g_x^I(\theta) + \frac{K_{II}}{\mu_0}\sqrt{\frac{r}{2\pi}}g_x^{II}(\theta) \\ & + u_{x0} - \omega_0 r\sin(\theta) \\ & + \frac{r}{2\mu_0}\{C_2(\kappa+1)\cos(\theta) + D_2(\kappa+1)\sin(\theta)\} \\ & + O\left(r^{3/2}\right) + \ldots, \end{aligned} \tag{2}$$

$$\begin{aligned} u_y = {} & \frac{K_I}{\mu_0}\sqrt{\frac{r}{2\pi}}g_y^I(\theta) + \frac{K_{II}}{\mu_0}\sqrt{\frac{r}{2\pi}}g_y^{II}(\theta) \\ & + u_{y0} + \omega_0 r\cos(\theta) \\ & + \frac{r}{2\mu_0}\{C_2(\kappa-3)\sin(\theta) - D_2(\kappa+1)\cos(\theta)\} \\ & + O\left(r^{3/2}\right) + \ldots, \end{aligned} \tag{3}$$

where μ_0 is the shear modulus at the crack tip. For generalized plane stress conditions, applicable to most experimental cases, $\kappa = (3-\nu)/(1+\nu)$. Functions of θ are identical to those describing the behavior of homogeneous materials [14]. In the above, one can readily recognize the characteristics of a homogeneous crack associated with the first two powers of r. The influence of nonhomogeneity appears in the subsequent terms. By inference, the first two terms of the stress field are also devoid of nonhomogeneity. Only the local material properties pertaining to the crack tip position enters the equations. These do not, however, preclude the need for the higher order terms, as local plasticity, triaxiality, and singularity inherent to the immediate vicinity of the crack tip often prevents extraction of experimental (optical) data within that region. Thus, this solution can only be embraced with caution in experimental cases. , Using exponential variation of Young's modulus, Parameswaran and Shukla [15] developed the asymptotic expansion of quasi-static crack-tip stress fields for a crack aligned with the direction of property variation. On similar lines, Chalivendra et al. [16] derived mixed-mode crack-tip stress fields for a crack inclined to the exponential elastic gradation. Jain et al. [17] continued analytical studies in FGMs by developing

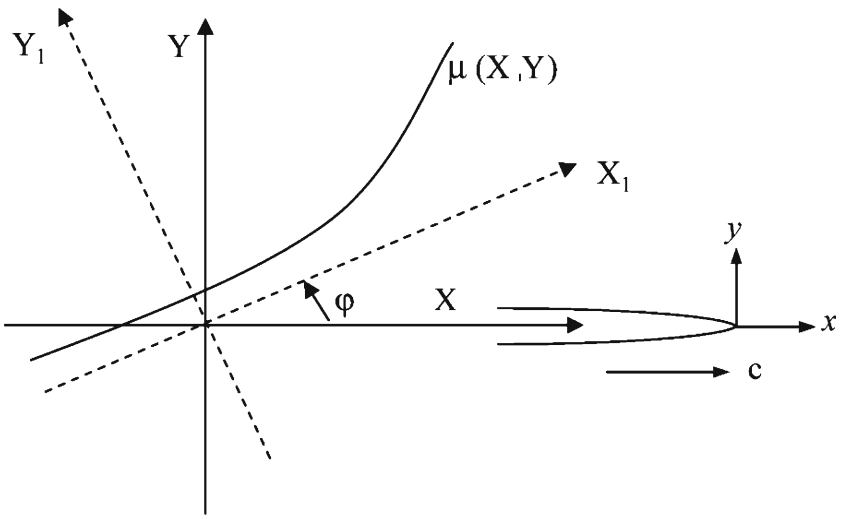

Fig. 1 Propagating crack orientation with respect to direction of property variation in FGM

both mode-I and mixed crack-tip field equations for linearly varying property variation. Recently, Chalivendra [18, 19] developed quasi-static crack-tip field equations for a crack in orthotropic nonhomogeneous solids using scaled coordinates approach proposed by Krenk [20]. For brevity, the authors consider a typical case of linear variation of Young's modulus at an angle to property gradation as shown in Fig. 1 and the variation is expressed by:

$$E(X, Y) = E_0 (1 + \beta X + \gamma Y), \tag{4}$$

where E_o is Young's modulus value at the crack tip, β and γ are nonhomogeneity coefficients dependent on property gradation angle φ shown in Fig. 1. The compatibility equation in terms of Airys stress function for plane stress conditions takes the following form:

$$\begin{aligned}&(1+\beta X+\gamma Y)^2 \nabla^2\left(\nabla^2 F\right) - 2\beta (1+\beta X+\gamma Y)\\ &\cdot\frac{\partial}{\partial X}\left(\nabla^2 F\right) - 2\gamma (1+\beta X+\gamma Y)\cdot\frac{\partial}{\partial Y}\left(\nabla^2 F\right)\\ &+2\left(\beta^2+\gamma^2\right)\left(\nabla^2 F\right) - 2(1+\nu)\\ &\cdot\left(\beta^2\frac{\partial^2 F}{\partial Y^2}+\gamma^2\frac{\partial^2 F}{\partial X^2}-2\beta\gamma\frac{\partial^2 F}{\partial X\partial Y}\right)=0,\end{aligned} \tag{5}$$

where $\nabla^2 = \frac{\partial^2}{\partial X^2} + \frac{\partial^2}{\partial Y^2}$. It may be observed from the above equations that if nonhomogeneity coefficients are set to zero, the equation reverts to the standard biharmonic equation for homogeneous materials. The nonhomogeneity coefficients make the solution process complex and the solution for equation (5) is obtained through an asymptotic analysis coupled with Westergaard's stress function approach [21]. The details for the derivation of the solution of Airys stress function and the crack field equations can be found in Jain et al. [17]. The normal stress in the y-direction being the most prominent, the focus will be briefly shifted towards it in an attempt to gain insight into the stress field characteristics of FGMs. The equation is described as:

$$\begin{aligned}\sigma_{yy} = \sum_{n=0}^{1}&\Big[\Re\{P_n\} + y\Im\{P_n'\} - y\Re\{R_n'\} + y\Im\{Q_n'\}\\ &+ \Im\{S_n\} - y\Re\{S_n'\}\Big] + \beta\left[\frac{-y^2}{2}\Re\{P_0'\} - \frac{y^2}{2}\Im\{R_0'\}\right.\\ &\left.- \frac{y^2}{2}\Re\{Q_0'\} - \frac{y^2}{2}\Im\{S_0'\}\right] + \gamma\left[\frac{y^2}{2}\Im\{P_0'\}\right.\\ &\left.- \frac{y^2}{2}\Re\{R_0'\} + \frac{y^2}{2}\Im\{Q_0'\} - \frac{y^2}{2}\Re\{S_0'\}\right].\end{aligned} \tag{6}$$

The variables P, Q, R, and S in the above equation are associated with powers of distance from the crack tip, r, with unknown coefficient whose numerical values can only be retrieved experimentally or numerically. These functions are commonplace in homogeneous analysis [21], with P_0 and R_0 exhibiting the well-known square-root singularity for modes I and II, respectively, and their coefficients representing the stress intensity factors K_I and K_{II}.

Clearly, the prominent terms that involve singular characteristics are devoid of the influence of nonhomogeneity. The term involving the T-stress also remains unaltered. Only those beyond $r^{1/2}$ power term are affected by the material nonhomogeneity. It is finally observed that mode mixity will not be a factor unless material variation is asymmetric with respect to the crack direction.

A more experimentally adaptable problem was later studied by Erdogan and Wu [22]. Indeed a surface crack normal to a boundary has been frequently the subject of experimental investigation under various configurations such as modified compact tension (MCT), single-edge notch tension (SENT), under three- or four-point, or uniaxial loading conditions, amongst others. The specific analytical solution includes the inherent material properties variations, and the stress intensity factor is found to be directly coupled with the elastic modulus $\mu(x)$. The predictive behavior of FGMs with variations of a decade between increasing and decreasing Young's modulus gradients reveals a doubling in the value of normalized stress intensity factor.

Using the asymptotic analysis, theoretical crack tip expressions were first obtained for both exponential and linear variation of mechanical properties by Parameswaran and Shukla [23] for all three modes of dynamic fracture in graded materials. Chalivendra et al. [24] developed higher order mixed-mode crack tip stress field equations for a crack propagating at an angle to the property gradation direction. Subsequently, Shukla and Jain [25] and Lee [26] obtained crack-tip stress field equations using displacement potentials for a crack propagating in FGMs.

For a typical case of exponential variation of shear modulus, Lamé's constant and mass density considered by Parameswaran and Shukla [15], the equations of motion takes the form:

$$\begin{aligned}&\nabla^2\Delta + \beta\frac{\partial\Delta}{\partial X} - \beta\left(\frac{\kappa-1}{\kappa+1}\right)\frac{\partial\omega}{\partial Y} = \left(\frac{\kappa-1}{\kappa+1}\right)\frac{\rho_0}{\mu_0}\frac{\partial^2\Delta}{\partial t^2}\\ &\nabla^2\omega + \beta\frac{\partial\omega}{\partial X} - \beta\left(\frac{3-\kappa}{\kappa-1}\right)\frac{\partial\Delta}{\partial Y} = \frac{\rho_0}{\mu_0}\frac{\partial^2\omega}{\partial t^2},\end{aligned} \tag{7}$$

where $\kappa = (3 - 4\nu)$ for plane strain, and the relation for plane stress given by $\kappa = (3 - \nu)/(1 + \nu)$; ν is the Poisson's ratio; $\Delta = (\partial u/\partial X) + (\partial v/\partial Y)$ is the dilatation and $\omega = (\partial v/\partial X) - (\partial u/\partial Y)$ is the rotation; μ_0 and ρ_0 are the shear modulus and mass density at the origin; β is the nonhomogeneous factor. The above equations would reduce to the classical 2-D wave equations of dilatation and rotation by assigning β a value of zero. Due to nonhomogeneity, these equations lose their classical form and remain coupled in two fields Δ and ω, through the nonhomogeneity parameter β. Again, using an asymptotic approach, they provided a direct expression for the first stress invariant, though individual stress components may be derived from their formulation. The expression is provided for the $-1/2$, 0, and 1/2 powers of r, and is reproduced here for the exponential case, when the elastic variation is along the crack orientation:

$$\begin{aligned}\sigma_{xx} + \sigma_{yy} = {} & 2(\lambda_c + \mu_c) \cdot e^{\beta x} \\ & \left\{ A_0 r_l^{-1/2} \cos\frac{\theta_l}{2} + A_1 \right. \\ & + A_2 r_l^{1/2} \cos\frac{\theta_l}{2} - \frac{\beta}{4\alpha_l^2} A_0 r_l^{1/2} \cos\frac{3\theta_l}{2} \\ & \left. + \frac{2\beta\alpha_s}{(k+2)\left(\alpha_l^2 - \alpha_s^2\right)} B_0 r_s^{1/2} \cos\frac{\theta_s}{2} \right\}, \end{aligned} \tag{8}$$

where

$$r_{l;s} = \sqrt{x^2 + \alpha_{l;s}^2 y^2}, \quad \tan\theta_{l;s} = \frac{\alpha_{l;s} y}{x},$$
$$\alpha_l = \sqrt{1 - \frac{\rho_0 c^2}{\mu_0 (\kappa + 2)}}, \quad \alpha_s = \sqrt{1 - \frac{\rho_0 c^2}{\mu_0}},$$

λ_c and μ_c are the local (crack-tip) values of the Lamé's constant and shear modulus, respectively; ρ is the material density, c is the crack speed, and κ is the ratio of the Lamé's constant to the shear modulus. Note that just as in the work of Erdogan and Wu [22], the exponent characterizing the material variation appears outside the expansion, as an external factor. The asymptotic expansion itself follows the homogeneous model.

Recognizing that cracks could experience highly transient conditions during growth, Jain and Shukla [27] and Chalivendra and Shukla [28] obtained transient stress and out-of-plane displacement fields, respectively, for cracks propagating in FGMs. Recently, Chalivendra [29] has also derived transient crack-tip out-of-plane displacement field equations for cracks propagating along a gradually varying curved path in FGMs, and Lee et al. [30] has developed thermo-mechanical stress fields for propagating cracks in graded materials. In favor of brevity, these equations are not reproduced here due their extended nature. Instead, they are presented in an abridged form as they are utilized directly in the analysis of experimental data. The reader is thus referred to a later section on dynamic mixed-mode crack propagation.

The studies pertaining to the mode-III fracture of FGMs have also been numerous (e.g., [22, 31–37]) and have proven useful to understand the structure of crack tip fields in FGMs. The latest effort in the arena is attributed to Kubair et al. [38] who have provided an asymptotic solution to the problem of an inelastic FGM whose property variation is describable by a power law. Just as is the case for the other two modes of fracture, the stress variation is again shown to have the standard square-root of r singularity and retain a form identical to that of the homogeneous case. The second term in the expansion invokes the material property gradation. However, unlike the other solutions, the coefficient of the second term is fully defined in an unusually dependent relation to the first term. As mode-III problems are difficult to simulate experimentally, verification of this and other solutions is yet to be undertaken.

Quasi-static Experimental Investigations

Crack Perpendicular to the Direction of Gradation

Material system I

Butcher et al. [8] have published the first set of fracture experiments performed on FGMs with a continuous compositional gradation. The reader is directed to the original publication for details necessary to permit duplication of the material. Briefly, the method is based on a gravity assisted scheme wherein solid A-glass (soda-lime) spheres of mean diameter of ~40 μm are mixed into a slow curing epoxy. The mixture is poured into a mold for preparing uniform thickness (5.5 mm) sheets of FGM. Gravity draws the heavy glass particles to the bottom of the mold, whereas the lighter epoxy rises to the surface. Concurrent gelation of the composite guards against complete segregation of the two constituents, resulting in a three-fold *continuous*, and *semi-linear* variation in elastic modulus (2,800 MPa $< E <$ 8,500 MPa) over a range of 40 to 50 mm. Additional physical properties of these materials are listed in Table 1. For comparative purposes, those of other materials systems discussed in this paper are also presented in the table.

For conducting experiments, specimens 125 mm long and 24 mm high were manufactured from cast sheets, with gradation along the largest dimension of the specimens. Edge cracks of length 5.5 mm (150 μm width)

Table 1 Comparison of physical properties of FGM material systems

Material system	Young's modulus E (MPa)	Poisson's ratio ν –	Fracture toughness K_{Ic} (MPa $\sqrt{m}$)	Density ρ (kg/m^3)	Gradation range (mm)
I	2,800–8,500	0.37–0.33	1,400–2,200	1,150–1,850	40
II	160–250	0.45	1.8–0.8	960	150
III	3,600–5,200	0.33–0.43	470–800	1,200–950	250

were introduced at different locations along the length of the specimens, perpendicularly to the gradation, and the specimens were loaded in a three-point bend configuration. Also, the specimens were made specularly reflective in the region of interest by depositing an aluminum film onto the specimen surface to perform interferometric measurements.

Experimental method I: description of interferometer

The optical method of reflection-mode coherent gradient sensing [39], was used to map crack tip deformations. The schematic in Fig. 2 illustrates the experimental set up.

A collimated beam of light is incident on the specimen surface through a beam splitter. The reflected light beam (or the object wave front) carries the information about the surface non-planarity as a result of deformations near the crack tip. The angular deflections of the light rays relative to the optical axis are then measured as interference fringes by a wave front shearing apparatus consisting of two Ronchi gratings of identical pitch with grating lines parallel to the y-direction (horizontal) for wave front shearing in the x-direction (vertical, coincident to the plane of the crack). The gratings are physically separated along the optical axis by a distance Δ, to shear the wave fronts laterally in discrete directions depending on the grating pitch and the wave length of the light used. These wave fronts are collected by a positive lens of a camera and diffraction spots are displayed on the back focal plane of the lens. By filtering either the $+1$ or -1 diffraction spots, the optical fringe patterns representing contours of constant $(\partial w/\partial x)$ can be imaged. Mathematically, the governing equation of the technique is expressed by,

$$\frac{\partial w}{\partial x} = \frac{Np}{2\Delta}, \quad N = 0, \pm 1, \pm 2 \ldots, \tag{9}$$

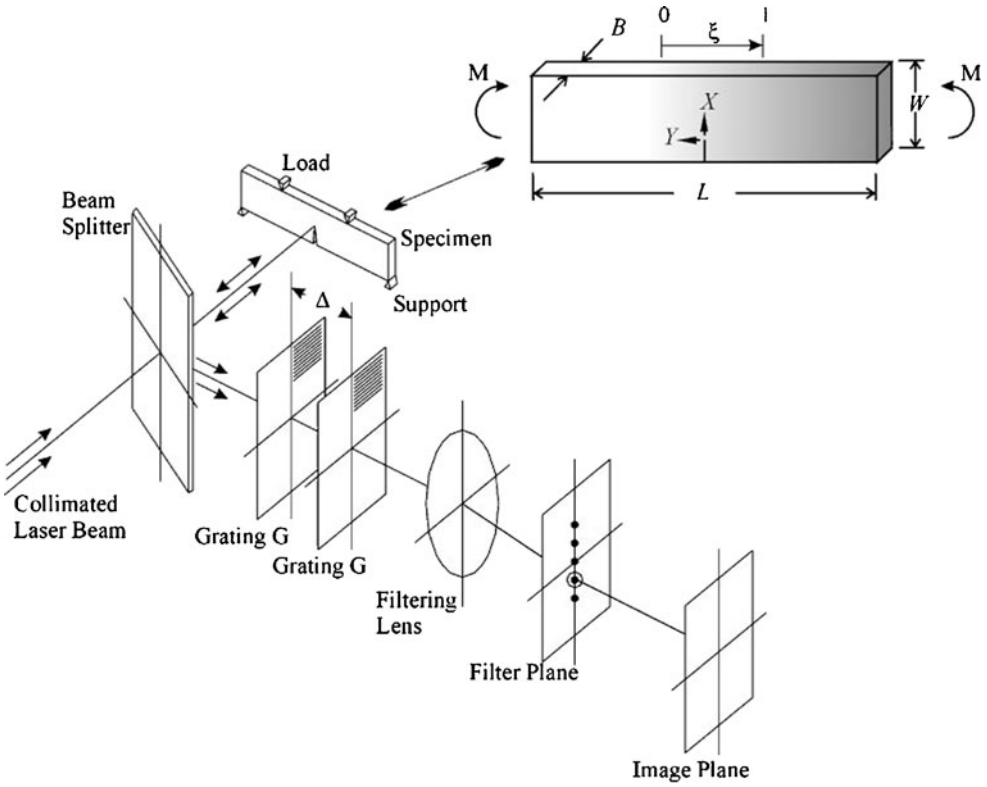

Fig. 2 Schematic of functionally graded beam and reflection CGS optical set-up used for mapping crack tip deformations [40]

where N denotes the fringe orders, p is the grating pitch (25 μm), and Δ is the grating separation distance (43 mm), resulting in an approximate sensitivity of 0.008° per half-fringe.

Designating the specimen thickness as B, the out-of-plane displacement w is related to the in-plane stresses as follows:

$$\frac{2w}{B} = -\frac{\nu}{E}\left(\sigma_x + \sigma_y\right). \tag{10}$$

Therefore, the stress formulations posed in the previous section can be used to extract fracture parameters such as stress intensity factors K_I and K_{II}. Note that for an accurate estimation of stress intensity factors using 2-D linear elastic K-dominant theories the data in the range of $0.4 < r/B < 0.7$ and $90° < \theta < 135°$ [39] is preferable.

Analysis of interferometric data

The experiments of Butcher et al. [8] featuring cracks normal to the direction of gradation were quickly extended by Rousseau and Tippur [40], who also compared fracture responses of homogeneous and bimaterial specimens with those of FGMs. Cracks were placed at locations $\xi = 0, 0.17, 0.33, 0.58, 0.83$, and 1 along the graded region of the specimen. The variable ξ represents the fraction of distance from the most compliant location ($\xi = 0$: pure epoxy, corresponding to elastic modulus E_1) to the stiffest location ($\xi = 1$: 52% volume fraction of spherical beads in the epoxy matrix, corresponding to elastic modulus E_2). Homogeneous experiments were conducted, respectively, at both of these extremes, while the bimaterials were generated by conjoining independent specimens with properties E_1 and E_2.

Interferograms for two FGMs, a bimaterial, and a homogeneous material are presented in Fig. 3. A pronounced fringe asymmetry relative to the crack is evident for the bimaterial. It is far weaker, yet perceivable in case of FGMs, in the form of a fringe tilt toward the compliant region (left side). This asymmetry occurs in spite of the symmetric loading used in these experiments.

In this work, the analysis of the optical data considered solely the singular term which depended only on

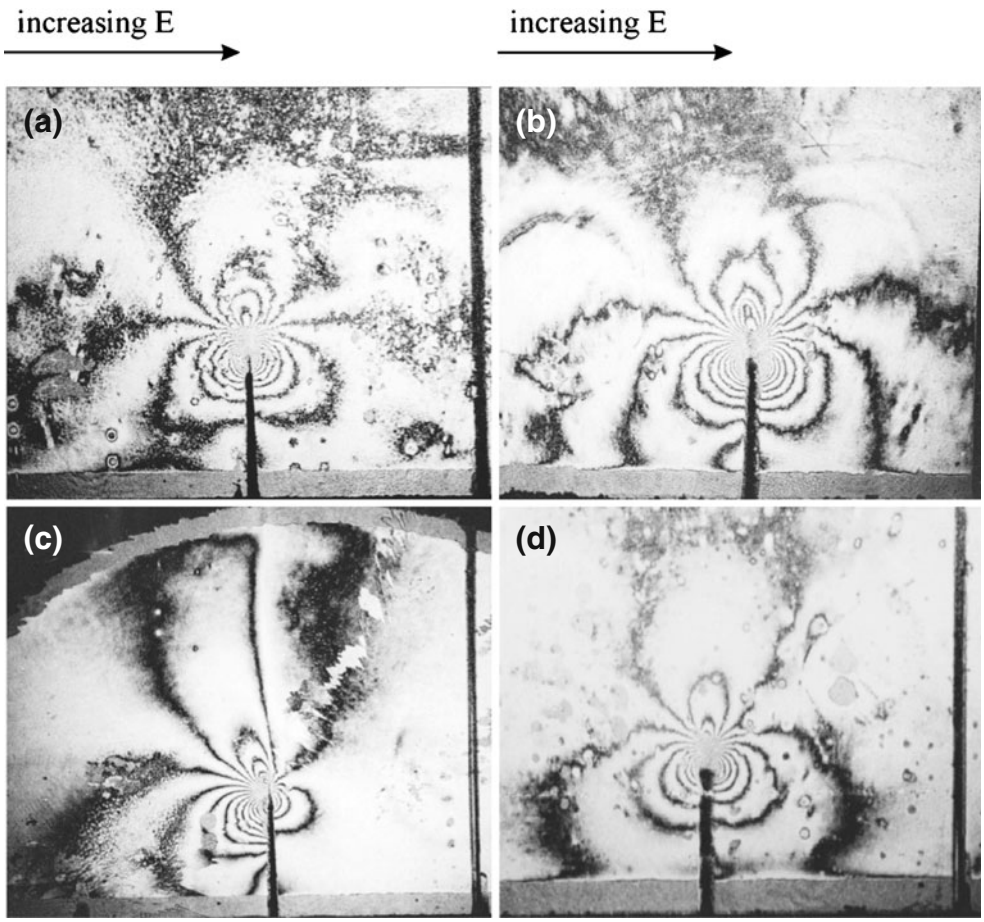

Fig. 3 Crack tip interference representing contours for FGMs with ξ equal to (**a**) 0.33, (**b**) 0.58, (**c**) bimaterial ($V_f = 0$,0 and 0.5), and (**d**) homogeneous glass/epoxy composite ($V_f = 0.5$) [40]

the local properties at the crack tip, and did not include the influence of the gradation parameters. Companion finite element analyses were executed to evaluate stress intensity factors that agreed with the experimental results closely, thereby reinforcing the notion of dominance of singularity in cases where the crack crosses the path of the gradation. The results also showed that for such cracks, the stress field becomes inherently mixed mode with material deformation heavily shouldered by the compliant regions of the specimen.

These experiments also highlighted the superiority in performance of FGMs when compared to comparable bimaterials. As illustrated by Fig. 4, for similar magnitudes of loading, the energy release rates for FGMs, normalized by the local fracture toughness at the crack tip, fall consistently below those of bimaterials by at least a factor of 3. However, the apparent deficiency of the bimaterials cannot be attributed to interfacial weakness, as FGMs with cracks located at $\xi = 0$ and 1 could only be achieved by bonding, thereby the insertion of an artificial interface identical to that of the bimaterials. Also, comparative assessment between FGMs, which can also be inferred from Fig. 4, suggests that more favorable conditions exist when the crack is located on the stiffer side of the gradient.

As cracks extend in such FGMs, the material asymmetry gives rise to crack kinking, as shown in Fig. 5. Based on assumption of local crack homogeneity in FGMs, as formulated by Gu and Asaro [41], predictions of kink angle were plotted and compared with numerical as well as experimental measurements. All three techniques compared favorably showing a greater

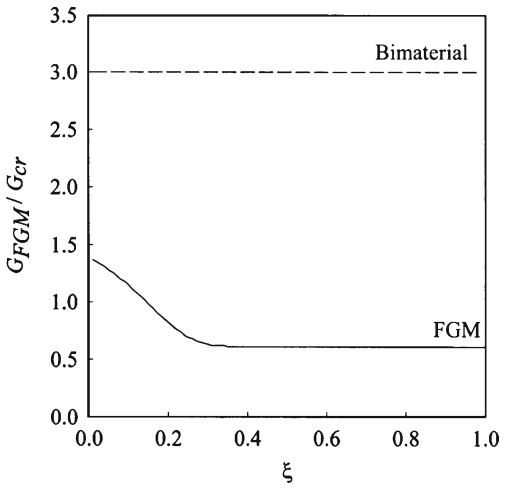

Fig. 4 Variation of energy release rate with ξ for FGM with $a/W = 0.3$ normalized by the corresponding critical values of energy release rate [40]

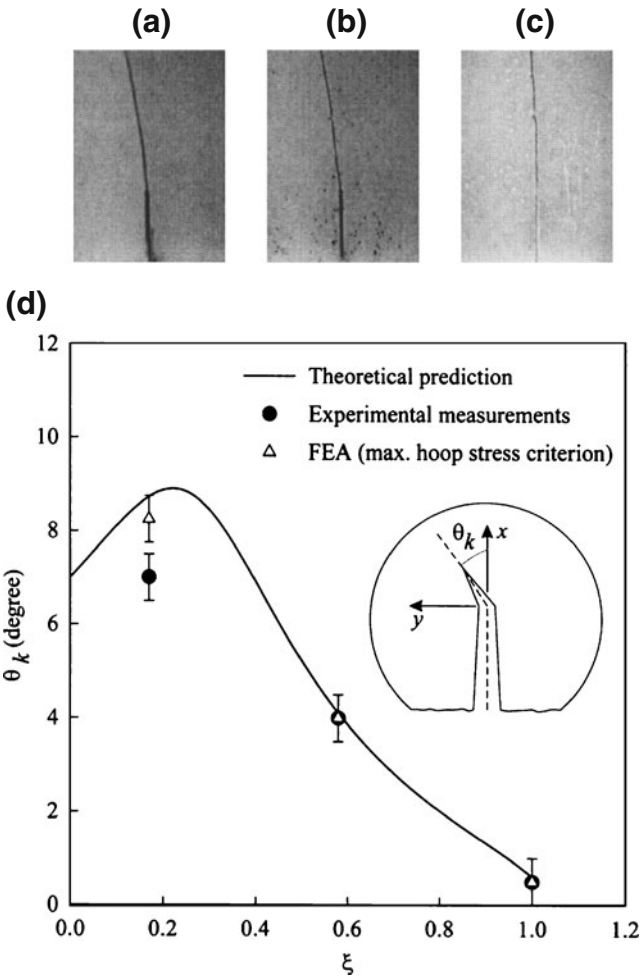

Fig. 5 Crack kinking angle in FGMs at ξ equal to (**a**) 0.17, (**b**) 0.58, and (**c**) 1.00; (**d**) variation of kink angle at all ξ locations for FGM with $a/W = 0.25$ [40]

kinking tendency as a crack is situated closer to the compliant end of the material.

Understanding of crack kinking in FGMs was further advanced by Abanto-Bueno and Lambros [42] by inserting an inclined crack with respect to the direction of gradation. However, before discussing their contribution, the model FGM material they have developed and the experimental technique they have used are first described in the following.

Material system II

Lambros et al. [43] have devised a way of preparing continuous FGMs for experimental modeling without using different constituents. The base material used for this purpose is polyethylene co-carbon monoxide (also known as ECO plastic), which undergoes degradation when irradiated with ultraviolet (UV) light. The

resulting molecular alteration results in the material becoming stiffer and stronger but more brittle. They prepared specimens by placing in a UV irradiation chamber. The shield was linked to a stepping motor that gradually but continuously displaced it, exposing the specimen underneath for durations ranging between 5 and 122 hours, depending on the desired type of gradation. They have achieved up to a 1.5 fold increase in elastic modulus, relative to the unaltered ECO having a value of $E = 160$ MPa.

Experimental method II: description of digital image correlation

The 2D Digital Image Correlation (DIC) method scrutinizes the material surface from which in-plane displacements and strain between two consecutive loading states can be derived. The technique, originally introduced by Peters and Ranson [44] and subsequently developed by Sutton and co-workers [45], is a full-field measurement method. Briefly, it consists of either making use of surface texture, or introducing superficial random speckles onto the specimen being investigated. Subsequent comparison and monitoring of speckles between two states of stress yield displacements and hence strains.

Data analysis of DIC

The uniqueness of the work carried out by Abanto-Bueno and Lambros [42], and later by Oral et al. [46] includes the introduction of mode-mixity by successively varying the direction of material gradation with respect to the placement of the crack. Furthermore, in addition to the generalized maximum hoop stress criterion used by Rousseau and Tippur [40], they have appended additional terms corresponding to the influence of the T-stress, giving rise to the relation:

$$K_I \sin\alpha + K_{II}\,(3\cos\alpha - 1) - \frac{16}{3} T\sqrt{2\pi r_c}\sin\frac{\alpha}{2}\cos\alpha = 0, \tag{11}$$

which includes a parameter r_c related to the microstructural length scale of the materials.

The FGM is incrementally loaded, and values of stress intensity factors, along with T-stress are obtained by inserting the DIC generated displacements into equations (2) and (3) and simultaneously solving the equations using a Newton–Raphson approach. A typical post-initiation and post-kinking image from their work for an FGM is shown in Fig. 6. In addition to the conspicuous crack opening, the decorated speckles are also clearly visible on the surface of the specimen.

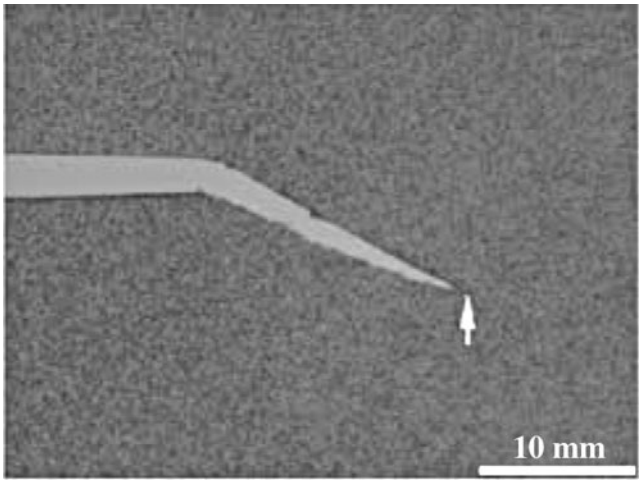

Fig. 6 Representative digital images recorded during the fracture tests, with crack tip location identified by arrow [42, 46]

Based on the results they note that withholding or including the T-stress term in the data analysis could have as much as 8% error in fracture parameters in case of homogeneous materials, inferring the need for its inclusion in FGMs. They also note that in homogeneous materials, crack growth criteria are solely guided by the maximum hoop stress. In FGM, on the other hand, the region of lower fracture toughness seems to also promote kinking towards it. Thus, although the prediction proved accurate to a maximum of approximately 20%, an additional criterion based on local failure properties is necessary for establishing a comprehensive FGM crack kinking rules.

Crack Parallel to the Direction of Gradation

Using the same material and optical techniques employed in the study of crack kinking, Lambros et al. [43] and Li et al. [47] investigated the quasi-static fracture behavior of ECO-based FGMs with edge cracks in the direction of gradation when loaded in pure mode-I configuration. The optical images were collected at a rate of 60 frames/s and used in concert with the 2D DIC technique to obtain full-field displacements. The experimental boundary conditions and measurements were then supplied to a finite element model, wherein a modified J-integral formulated for FGMs [48] was used to retrieve energy release rate and stress intensity factor of the loaded material. This hybrid method produced considerable success, as it resulted in a maximum difference of 12% with the exact solution of Erdogan and Wu [22]. They also studied conditions leading to crack initiation, and concluded that it is primarily dictated by the ability of the crack to accumulate enough

energy, allowing it to exceed the local critical value at the crack tip. Finally, the monotonic increase in the magnitude of stress intensity factor or energy release rate with crack length, observed by these researchers, appears to be universal, as this also holds true for non-homogeneous and bi-materials featuring crack normal to the gradient direction [40].

K-dominance in FGM

Experiments aimed at reaching a similar understanding of crack tip stress field when the plane of the latter lies in the direction of gradation were performed by Rousseau and Tippur [49]. The method of CGS, discussed previously, was used in their evaluation. Cracks were alternatively placed in the compliant and the stiff regions, respectively, and only a K-dominant formulation was used in the analysis of the interferograms. The latter are not reproduced here for they display similar demeanor to those of the homogeneous case presented in Fig. 3. Nevertheless, qualitative deviations from the homogeneous case are noticeable. When the crack is located on the stiff side of the gradient (decreasing gradient, or $E_2/E_1 < 1$), frontal fringe lobes are prone to expansion, while having the crack on the compliant side (increasing gradient, or $E_2/E_1 > 1$) has the opposite effect. These qualitative differences translate into differences in the measured value of the SIF. As seen in Table 1, for identical loading and geometry, the FGM with decreasing gradient registers nearly a 40% increase in SIF, when compared to its inverted gradient configuration, an FGM with a crack pointing toward the direction of decreasing gradient. However, one may not view the former as an inferior configuration since crack tip moduli of the two cases also differ by about 40%. On the other hand, when each FGM is compared to its homogeneous counterpart, it is clear that the FGM with increasing gradient is better than its counterpart, whereas, the FGM with decreasing gradient performs relatively poorly compared to the equivalent homogeneous material.

Further comparisons were performed between the experimental results, on the one hand, and finite element simulations of the experiments and the analytical solution of Erdogan and Wu [22], on the other hand. Whilst the latter two are identical, the experimental results underestimates them by about 20%. This points to the deficiency of analyzing crack tip fields using a K-dominant description for certain types of FGMs (Table 2).

Quasi-static crack growth experiments were also performed by the same authors, the results of which are shown in Fig. 7. Despite a lower crack tip toughness or resistance for the case corresponding to the crack residing on the compliant side, this specific FGM is capable of sustaining higher load before fracturing than the FGM having a crack on the stiff side of the specimen. Following initiation, no increase in load is necessary to sustain crack growth.

The issue of K-dominance in FGMs was further addressed by Abanto-Bueno and Lambros [50] during an evaluation of quasi-static crack growth in their ECO-based FGM. The specimen was subjected to pure mode-I loading and its surface strains measured by the DIC technique. All their evaluations were conducted for cracks parallel to the gradient direction, and located on the stiffer and more brittle side of the gradient (decreasing gradient, or $E_2/E_1 < 1$).

It must be noted that their R-curve differs from the afore-mentioned results reported by Rousseau and Tippur [49]. Indeed, whereas the latter reported no increase in loading to sustain propagation, the ECO material necessitates higher levels of energy to achieve continued growth, thereby resulting in a monotonically increasing R-curve. This difference is likely due to the difference, in this case increase, in ductility of ECO which is essentially absent in glass-filled epoxy FGMs.

Returning to the subject of K-dominance, Abanto-Bueno and Lambros [50] found only a limited region capable of justifying this assumption. Thus, only an area 4 mm distant from the crack tip ($r/B = 0.13$) and within a sweeping angle between 90° and 135° on either side of the plane of the crack could be used to provide

Table 2 Comparison of analytical, numerical, and measured stress intensity factors [49]

Method of calculation	FGM $E_2/E_1 = 2.23$ $E_0 = 4.8$ GPa	Homogeneous $E_2/E_1 = 1$ $E_0 = 4.8$ GPa	FGM $E_2/E_1 = 0.41$ $E_0 = 6.8$ GPa	Homogeneous $E_2/E_1 = 1$ $E_0 = 6.8$ GPa
FEA (plane stress, $\nu = 0.32$ or 0.34)	1.27	1.51	1.77	1.46
Analytical (plane strain, ν unknown)	1.28	1.52	1.79	1.45
CGS; K-dominant description (plane stress, $\nu = 0.32$ or 0.34)	1.06	1.26	1.44	1.20

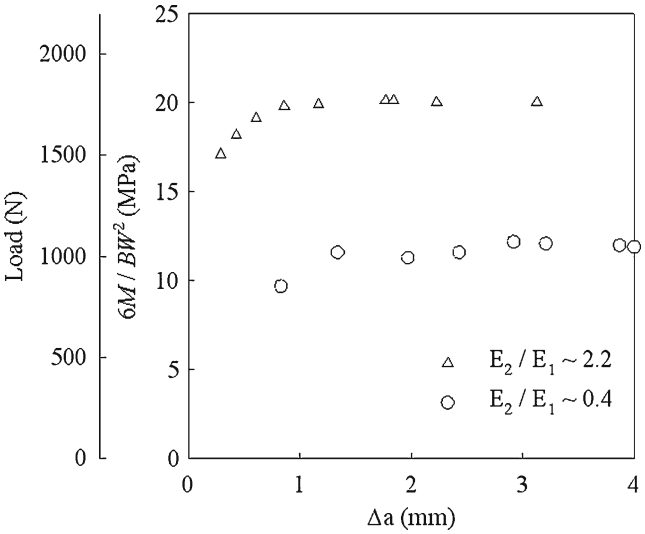

Fig. 7 Stress variation during slow crack propagation in FGMs with cracks initially at stiff and compliant edges, respectively [49]

results in good agreement with the theory formulated by Eischen [13], when only the first terms in expressions (2) and (3) were used.

Beyond K-dominance

Further investigation into the scope of equations (2) and (3) was performed by Abanto-Bueno and Lambros [51]. In particular, they focused on the influence of the constant C_2, the equivalent of the homogeneous T-stress. With a crack located in the ECO material with decreasing gradient, the displacement field was obtained using DIC and K_I and other parameters were obtained. These results were then used to regenerate the displacement fields [13], and compared to measurements. These results are shown in Fig. 8. In one case, the K-dominant term alone was used, only to expose its inability to correctly reproduce the deformation. The appendage of the sole T-stress merged the two fields quite well. Not shown in the figure is the addition of the second higher order term in the equations, which goes unperceived for this particular FGM.

Rousseau [52] attempted to refine the use of CGS in its use for studying crack tip fields in FGMs. In this work, the author presented asymptotic expansion of the first stress invariant for linearly varying elastic properties up to sixth terms. In this, every term becomes associated with the nonhomogeneous parameter β, either linearly or quadratically. The only term immune from its influence remains the dominant singular one ($r^{-1/2}$). Previously discussed interferograms from experiments using glass-filled epoxy composites were analyzed. It was found that the addition of each higher-order term resulted in improvement in the definition of surface

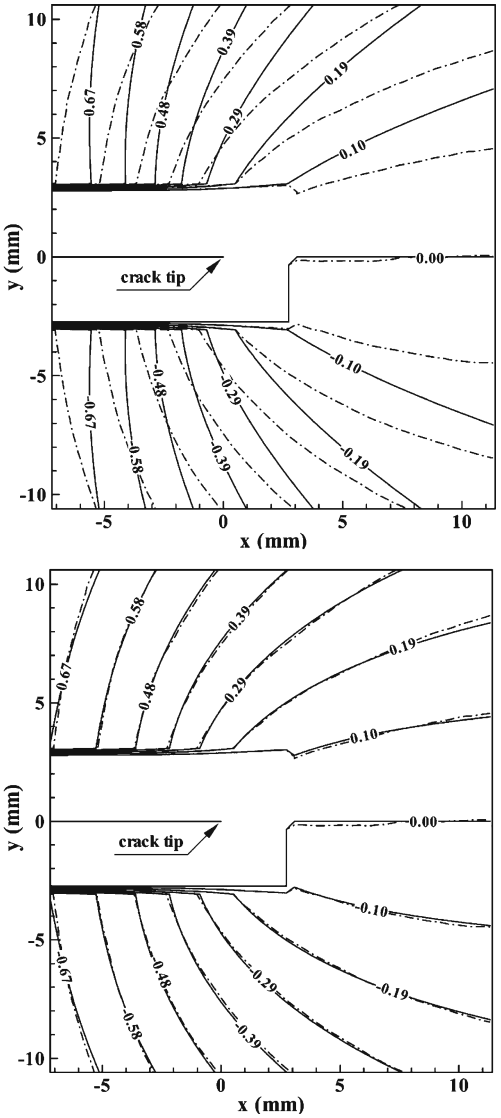

Fig. 8 Contour plots comparing measured (*dash-dotted line*) and theoretical (*solid line*) crack tip normal displacement fields as a function of the terms used to fit the displacement data. The terms used in the fitting, in addition to the two terms defining rigid body motion, were (**a**) K_I term and (**b**) K_I and C_{12} terms [51]

slope field, up to the third or fourth higher order term, depending on the direction of compositional gradation. The author also observed that FGMs with increasing elastic gradients are less prone to the effects of angular directionality, whereas the opposite FGM produces the best results within a span of $90° < \theta < 135°$. Interestingly, the same conclusion was also reached by Abanto-Bueno and Lambros [50] for their ECO FGM with $E_2/E_1 < 1$, as mentioned previously.

The influence of the higher-order terms is shown graphically by superimposing the analytical solution and experimental data (Fig. 9). The improved progression is presented for $n = 2$, 4, and 6, where a perfect fit is reached.

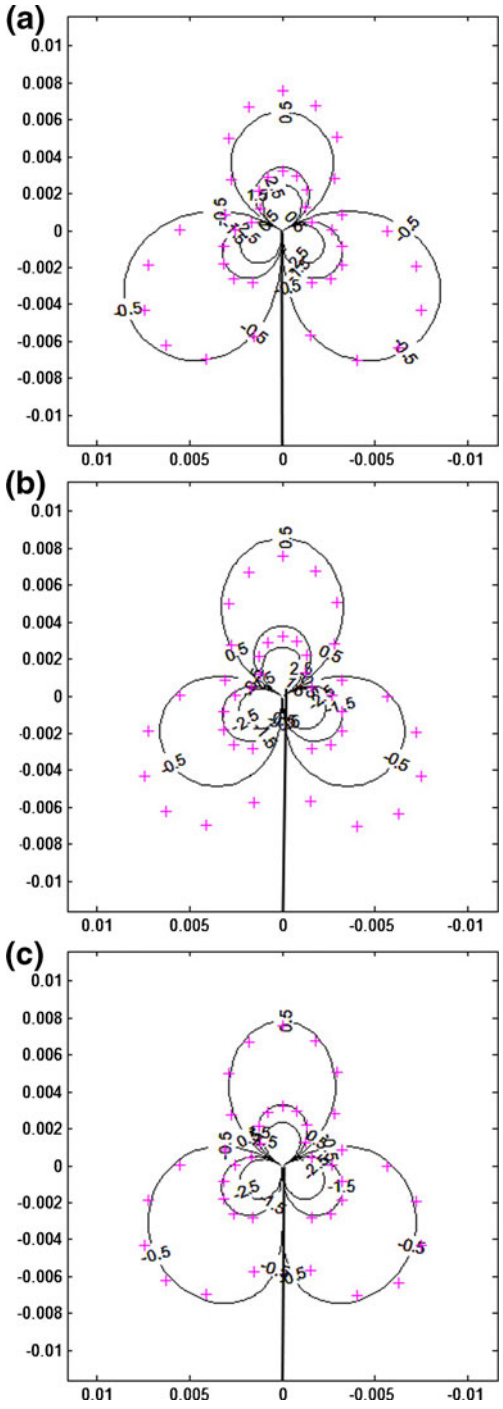

Fig. 9 Synthetic contours (*solid lines*) from multi-parameter, least-squares data analysis for specimen with crack located on stiff side of gradient: (**a**) $n = 2$, (**b**) $n = 4$, (**c**) $n = 6$. Crosses are periodic data obtained from experimental fringe pattern [52]

Dynamic Experimental Investigations

Mode-I Failure

The first dynamic experiments on FGMs were reported by Rousseau and Tippur [53]. These experiments were performed partly as a means of implementing the then recently-developed dynamic crack tip stress fields for FGMs (see equation (8)) [23]. The expressions related specifically to bodies assuming exponential shear modulus variations, but were in this case adapted to the linear variation present in the specimens under scrutiny. Previously mentioned material-system I was used in the experiments. Most properties of the material (elastic modulus, longitudinal and shear wave speeds, and density) increased quasi-linearly with compositional gradation. Only the Poisson's ratio followed the reverse trend.

Again, CGS was used to monitor surface slopes in the crack direction, both prior to and following crack initiation. A high-speed film camera was used to capture the event at a repetition rate of 5 μs. The loading mechanism consisted of a cylindrical steel impactor propelled towards the specimen edge, directly opposite the crack, at a speed of 5.3 m/s (see, insert of Fig. 10). This generated compressive stress waves that reflected at the opposite edge where crack was situated into a tensile stress wave that enshrouded the crack in a mode-I environment and eventually caused crack initiation.

Representative interferograms resulting from this type of loading will be presented later in this section. Before that some of the conclusions resulting from the analysis are discussed. Figure 10 shows the variations of the first stress invariant with respect to time. The magnitude of these stresses follow a generally increasing trend, indicative of a constant build up of strain energy at the crack tip. The homogeneous case is seen to be bounded by those for the two FGM cases, with the material with increasing gradient ($E_2/E_1 > 1$) be-

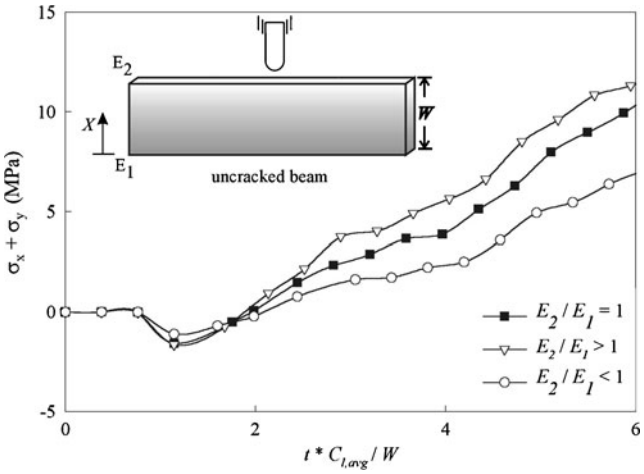

Fig. 10 $\sigma_x + \sigma_y$ at a location ($X = 0.2W, Y = 0$) in uncracked beams, with linearly varying elastic moduli, subjected to one point impact by a rigid projectile [53]

ing loaded at a higher rate in the prospective crack location. The crack in this FGM also propagates faster than the other two materials, which behave identically in their growth behavior. These two observations are significant particularly because as the volume fraction of the stiffer constituent in the FGM increases, the crack must overcome an environment of higher strength (higher S_y and S_u), stiffness (higher E), and toughness (higher K_{Ic}). This is also reinforced by the observation of the post-initiation stress intensity factor histories (Fig. 11).

The above study was complemented by similar evaluations on porous FGMs [54]. The same technique used for preparing material-system I was used in this case, but for the fact that the glass microspheres were hollow, and of such a low density that they gradually floated to the surface while the epoxy stagnated at the bottom. In addition, the average diameter of the inclusions was 60 μm, or approximately twice the size of the solid spheres. Comparatively, therefore, basic material properties assumed a trend which was the reverse of that of material I, i.e., decrease in density and stiffness with volume fraction. Otherwise, the experimental details were identical to those of the previous study.

The progression in a typical sequence of mode-I interferograms is shown in Fig. 12 during post-initiation period for $E_2/E_1 < 1$. Besides the obvious symmetry in fringe pattern relative to the crack, the unloading Rayleigh wave that originates from the initial crack tip at crack initiation is clearly visible. The stress field pertaining to the crack environment remains within its envelope, while contact stress conditions are at the top of the interferogram, beyond the cylindrical delineation

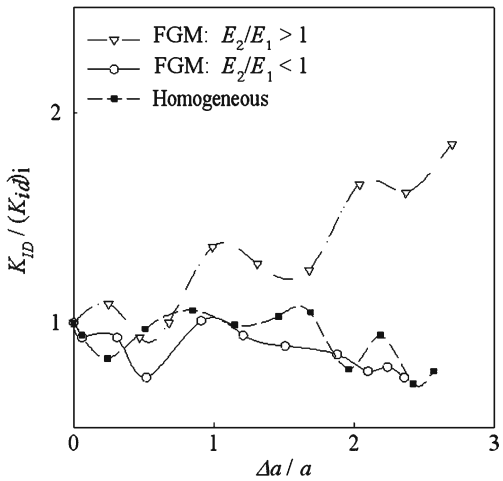

Fig. 11 Variation of apparent stress intensity factor with crack length [53]

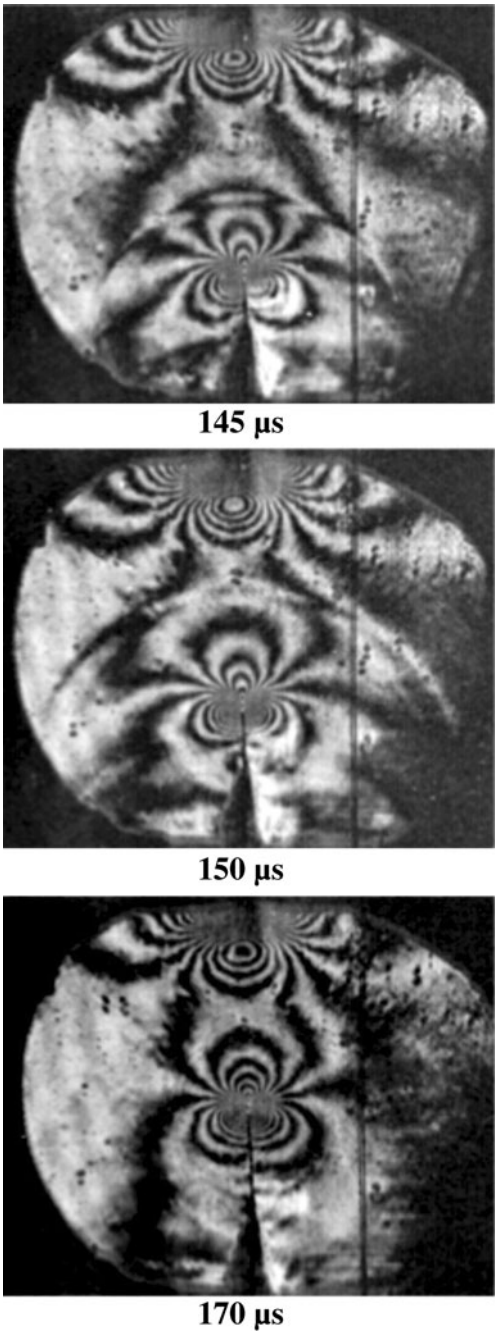

Fig. 12 Selected CGS interferograms representing contours of $\partial w/\partial x$ in functionally graded epoxy syntactic foam sheet with a crack on the stiffer side ($E_2/E_1 < 1$) impact loaded on the edge opposing the crack tip. Fringe sensitivity ~0.15 degrees/fringe, the vertical line parallel to the crack in each case is at a distance of 10 mm. Crack initiation time, t_i ~135 μs [54]

of the Rayleigh wave. As was the case in Rousseau and Tippur [53], the present results of the data analysis show a propensity for faster growth, higher K_I^d with increasing elastic modulus gradation. This concurrence of trends occurs in spite of the wide variation in particulate size, a three-fold difference in density and

elastic modulus, and the fact that in one case [53] the crack is moving into a particulate-rich environment while in the other case [54] the crack is moving away from such an environment, into a purely cross-linked thermoset region. It can therefore be concluded that elastic modulus variation takes precedence over microstructural differences in the dynamic fracture behavior of nominally brittle FGMs.

Sandwich Construction with a Graded Core

The versatility of material system I reinforced with hollow microballoons was extended from the previous studies to monitor its potential as a core material of sandwich structures. Thus Kirugulige et al. [55] devised two epoxy-based composites, both having identical epoxy face-sheets. The first was built upon a core of homogeneous microballoon-epoxy mixture. The homogeneous volume fraction ($V_f = 0.25$) was chosen so as to result in a material having the same elastic impedance, ρC, as a sandwich with an FGM core. The second core consisted of an FGM whose bilinear gradation varied from pure epoxy at the bottom to 45% microballoon V_f at its center, and again back to pure epoxy at the top. Furthermore, initial cracks were introduced so that local crack tip properties were identical in both materials. Both systems were impacted in a three-point bending configuration in pure mode-I, and their surface deformations measured using CGS. Equation (8) was used to analyze the interferograms.

Differences between the interferograms of the two materials are unremarkable. Likewise, the analysis of the various frames shows that crack initiation time and crack growth behaviors are almost identical. Furthermore, pre-initiation stress intensity factors in conventional and graded sandwiches could almost be superimposed upon each other. The sole difference in the behavior of the two materials appears after initiation. For the graded case, a marked decrease in the value of K_I^d is maintained during crack growth, primarily due to the decrease in local fracture toughness with increasing levels of micro-bubbles. The stress intensity factor continually decreases until the crack reaches center of specimen, at which point the trend reverses as the crack advances toward pure epoxy with higher toughness. More importantly, post-mortem inspection of the specimens reveals delamination of the face-sheet near the point of impact of the conventional composite, an occurrence not present in the FGM. Thus, it is evident that the FGM sandwich preserves the benefits of the conventional sandwich while suppressing potential interfacial delamination.

Mixed-Mode Failure

Mixed-mode dynamic failure in FGMs was investigated by Kirugulige and Tippur [56], using material-system I. This problem was solved analytically by Chalivendra and Shukla [28] and can be implemented for use with CGS as follows. Thus, CGS fringes representing surface slopes can be interpreted using [56],

$$\begin{aligned}\frac{\nu B}{2E}\frac{\left(\sigma_x+\sigma_y\right)}{\partial x} &= -\frac{\nu B}{2E}\\ &\cdot\Bigg[-\frac{1}{2}f\left(V;C_L,C_s\right)C_1\left(t\right)\cos\left(\frac{3\theta_l}{2}+\alpha\right)\\ &-\frac{1}{2}g\left(V;C_L,C_s\right)D_1\left(t\right)\sin\left(\alpha-\frac{3\theta_l}{2}\right)\\ &+\sum_{N=2}^{\infty}C_N\left(t\right)\left(\frac{N}{2}-1\right)r_l^{\left(\frac{N}{2}-2\right)}\\ &\cdot\cos\left\{\alpha+\left(2-\frac{N}{2}\right)\theta_l\right\}\\ &+\sum_{N=2}^{\infty}D_N\left(t\right)\left(\frac{N}{2}-1\right)r_l^{\left(\frac{N}{2}-2\right)}\\ &\cdot\sin\left\{\alpha+\left(\frac{N}{2}-2\right)\theta_l\right\}\Bigg]\\ &=\frac{Mp}{2\Delta},\end{aligned} \tag{12}$$

where (r_l, θ_l) denote crack tip polar coordinates associated with the growing crack tip along its instantaneous local direction. Functions f and g are associated with instantaneous crack velocity and are defined as:

$$\begin{aligned}f\left(V;C_L,C_s\right) &= \left(\frac{1+\nu}{1-\nu}\right)\frac{\left(1+\alpha_s^2\right)\left(1-\alpha_L^2\right)}{4\alpha_L\alpha_s-\left(1+\alpha_s^2\right)^2}\\ g\left(V;C_L,C_s\right) &= \left(\frac{1+\nu}{1-\nu}\right)\frac{2\alpha_s\left(1-\alpha_L^2\right)}{4\alpha_L\alpha_s-\left(1+\alpha_s^2\right)^2}\end{aligned} \tag{13}$$

where $\alpha_L = \left\{1-\left[\rho\left(1-\nu\right)V^2/2\mu\right]\right\}^{1/2}$ is associated to longitudinal waves, and $\alpha_s = \left\{1-\left[\rho V^2/\mu\right]\right\}^{1/2}$ corresponds to shear waves. The loading mechanism used in the experiments is as described in the earlier dynamic works, except that the crack is positioned eccentrically with respect to the loading point, simultaneously imposing a field containing the two in-plane modes. Typical interferograms, about 200 μs after impact, for both gradation directions are shown in Fig. 13. For an increasing gradient, the prevalence of pure mode-I is promptly recovered and faster crack propagation follows (upper interferogram). For the case of decreasing gradation

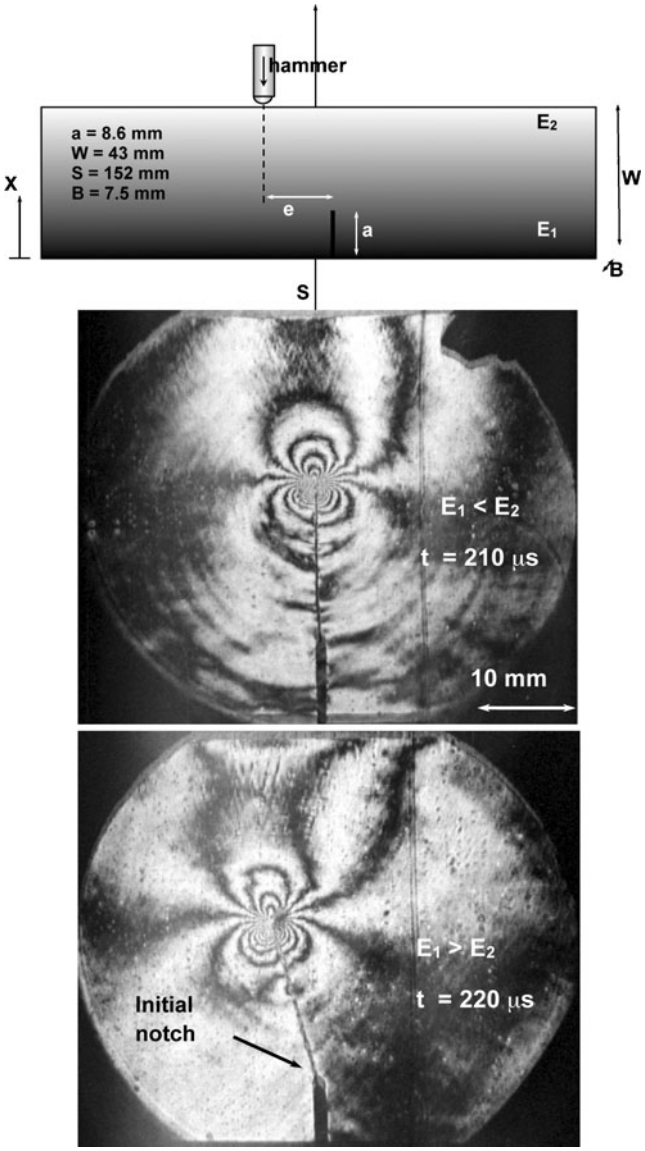

Fig. 13 Selected CGS interferograms representing CGS contours in FGM samples subjected to mixed mode loading

(lower interferogram) the incipient mixed-mode condition is maintained as illustrated by the asymmetry in size and orientation of fringe lobes. Also, this FGM is evidently prone to crack kinking. It was further found that as in the quasi-static case, the propagating crack appears to seek pure mode-I conditions, and follows directions corresponding to vanishing values of K_{II}. Nevertheless, it is noted that despite the high eccentricity of the imposed dynamic loading, the mode-II component of the response remains as a small portion of the overall stress field.

These experiments were further supported by the implementation of a finite element simulation wherein cohesive elements based on a bilinear traction separation law were dispersed within the broad vicinity of expected crack growth [57]. Good agreement was achieved with the experimentation, thereby providing further validation to the derived solution.

Material System III: Model FGM for Photoelasticity

Further experimentation on mixed-mode dynamic fracture of FGMs was performed by Jain and Shukla [58]. In their work, preparation of the graded material involved dispersion of cenospheres (made of aluminum silicate) within a polyester resin. (The cenospheres possess a far lower density than the matrix, and therefore, rise to the surface due to buoyancy before the polymer gels.) The resulting FGM had a decrease of 20% density from that of the pure matrix over a distance 250 mm. The material simultaneously showed a threefold increase in fracture toughness, accompanied by a linear 40% increase in elastic modulus.

Experimental Method III: Reflection Photoelasticity

A schematic of the experimental apparatus is shown in Fig. 14, and it shows essential elements of the dynamic photoelastic setup. A photoelastic coating (a birefringent sheet bonded to the FGM surface) is present on the specimen monitored using a circular polariscope during experiments. Note that photoelastic coating is absent along the plane of the crack. Rather, two separate photoelastic sheets are bonded on either side of the crack path where the optical data is measured. Disturbances to the light field due to optical anisotropy of the photo-elastic coating under stress are collected by a digital high-speed camera capable of recording 16 images at a rate of up to 200 million frames per second, with possible exposure time of 5 ns. The high optical sampling rate of the data provides the necessary resolution for accurate measurement of crack velocities. As the specimen is viewed through the circular polarizer, isochromatic fringes, which can be directly related to the stress level at any point in the specimen, are observed. The locations of constructive interference correlate to half-fringe orders, N ($N = \pm 1/2, \pm 3/2, \pm 5/2, \ldots$), whereas those where light is fully extinguished indicate integer values of N, ($0, \pm 1, \pm 2, \ldots$), or full fringe orders. The magnitude of maximum in-plane shear strains obtained from optical interference patterns is given by,

$$\gamma_{Max} = \varepsilon_1 - \varepsilon_2 = F_{CR}\frac{1+\nu^C}{E^C}\frac{Nf_\sigma}{2h^C}. \tag{14}$$

In the above, f_σ is the material fringe constant, h is the thickness of the coating, and N is the fringe order, ν is

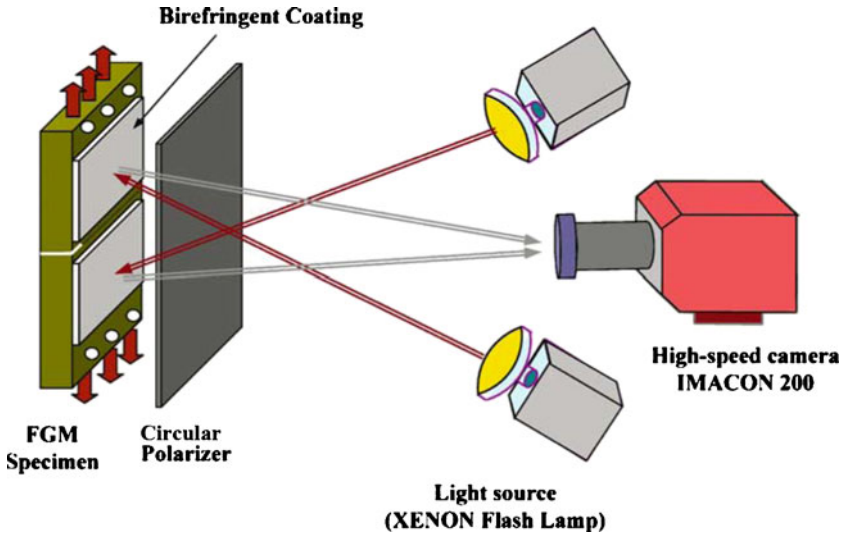

Fig. 14 Photoelastic configuration for testing FGM specimens [58]

the Poisson's ratio, and the superscript C refers to the coating, respectively. Also, in the above equation F_{CR} is a reinforcement correction factor that accounts for the fact that the coating carries a portion of the load.

Analysis of photoelastic fringes

A typical sequence of the isochromatic fringe patterns obtained using SENT specimens for cracks propagating parallel to the direction of material gradation is shown in Fig. 15. The photographs depict the dynamic stress field surrounding the crack tip as it propagates. In addition, the instantaneous location of the crack tip is indicated in each frame. The fringes correspond to crack propagation in the direction of increasing fracture toughness and increasing elastic modulus. Good symmetry of optical patterns relative to the crack is also observed suggesting mode-I deformations.

When the crack is rotated 30° with respect to the material gradation direction (Fig. 16), The isochromatics become asymmetric about the crack plane, an indication of mixed-mode loading at the crack tip.

The experiments were conducted for a homogeneous material and for FGMs, with cracks growing in the increase and decreasing gradient directions. All specimens were loaded to the same value of K_Q before crack initiation. The observations note different but constant crack-tip velocities in all cases, but lowest for the homogeneous material. This is different from the previously

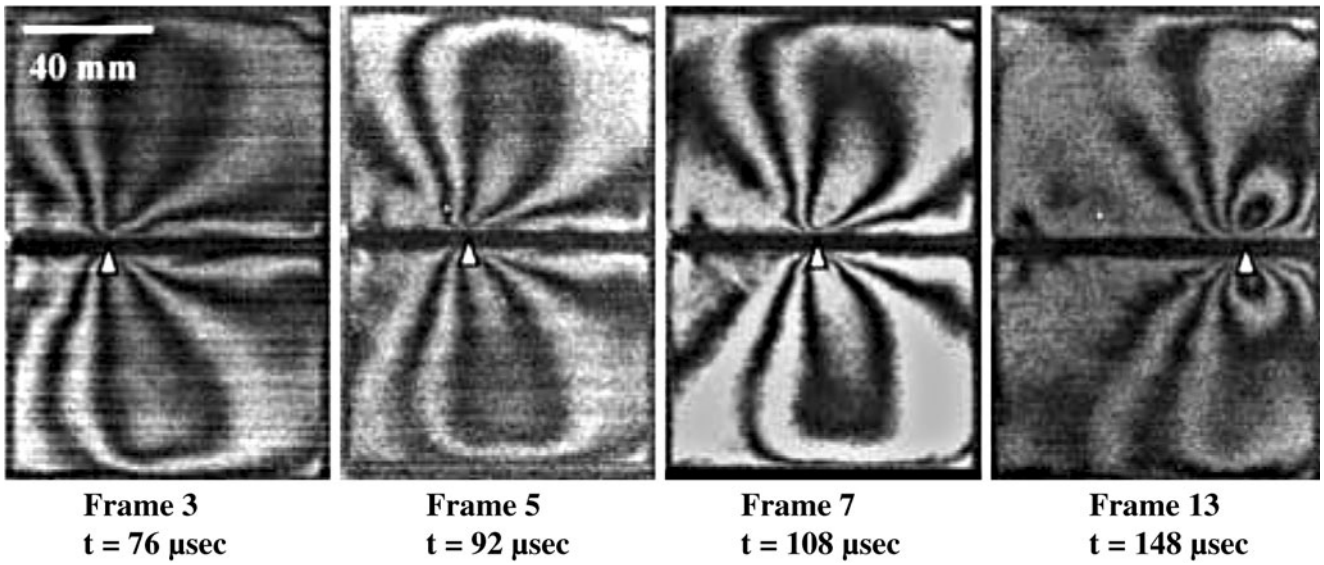

Fig. 15 Typical isochromatics obtained using SENT FGM specimens ($\varphi = 0$) (Crack tip is indicated by the triangle) [58]

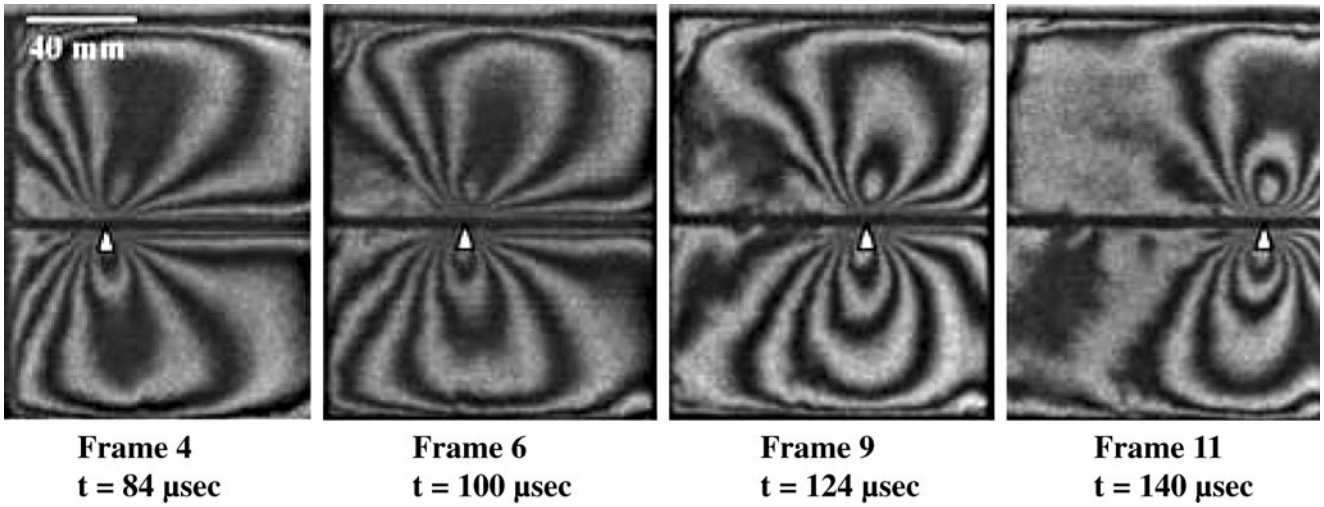

Fig. 16 Typical isochromatics obtained using SENT FGM specimens ($\varphi = 30°$) (Crack tip is indicated by the triangle) [58]

studied dynamic cases, possibly due to differences in the material systems. However, as before, the crack in FGMs with increasing gradient fractures faster than all other materials, reaching a speed equal to 62% of the Rayleigh wave speed. The authors attribute such high-speeds to weak interfaces between the cenospheres and polyester. Furthermore, larger crack angles with respect to compositional gradient have been shown to result in slowing of the propagating crack. Further, no crack kinking during the failure process was observed as a result of the material asymmetry.

The stress intensity factor histories are akin to those presented in Fig. 10 where locating the crack in the direction of increasing gradient requires higher levels of

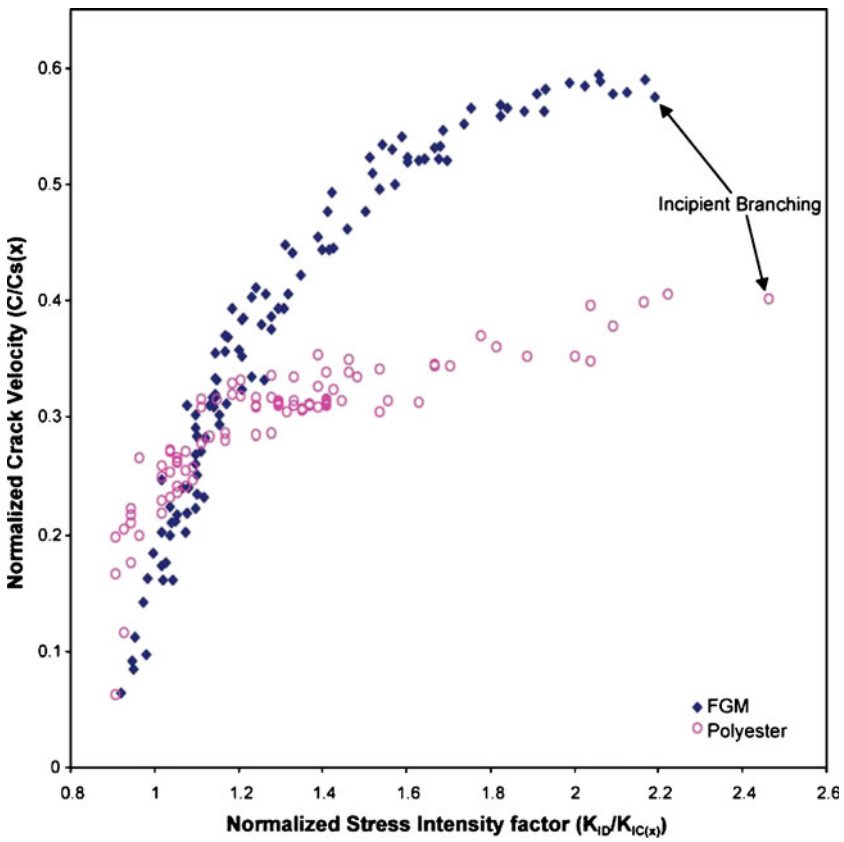

Fig. 17 Normalized crack velocity versus normalized-KID relationship for FGM and polyester [58]

energy to sustain constant velocities. This is the reverse of the FGM with decreasing gradient, which experiences multiple oscillations, but on the average retains a constant level. Here again, the authors reaffirm the prevalence of local fracture toughness as the dominant factor in the dynamic crack growth behavior of FGMs. The crack orientation also has the same effect on stress intensity factor as it does on speed; increasing angle lowers the overall magnitude of stress intensity factor history as the crack grows.

The relationships between crack velocity and dynamic SIF were established both for the homogeneous matrix and for FGMs with the pre-crack on the compliant side (Fig. 17). Three distinct domains exist in these plots: a vertical portion, the stem, which expresses independence between velocity and SIF in the low-velocity regime; a terminal, high speed, velocity region in which, significant increases in K_{ID} are required to produce small increases in the crack velocity; and a transition region connecting the stem and terminal velocity regions, referred to as the knee.

A key observation relates to the concept of crack arrest toughness, which is the SIF value at which a fast-running crack can be brought to rest before a catastrophic failure occurs. The local crack initiation fracture toughness, K_{IC}, is about 10% higher than the corresponding arrest toughness, K_{Im}, in both materials. As a stationary crack is loaded monotonically, the crack-tip is blunted and a plastic zone is formed. A propagating crack, however, is sharper and has a smaller plastic zone. Consequently, more energy is required to initiate fracture from a blunted, stationary crack than is required to maintain rapid propagation of a sharp crack. The crack arrest toughness is obtained from the curve fitting of experimental data points. The inability to directly obtain a K_{Im} value at a zero propagation velocity is due to the abrupt deceleration of the crack immediately prior to the arrest event. At such high rates of change, the inter-frame times of the high-speed camera cannot be set sufficiently low to capture a near-zero velocity pre-arrest event. The figure shows that propagation profile of the FGMs in the high-velocity region exceed that of the neat polyester by 50%.

Transient Effects

Dynamic crack tip field equations with transient effects for nonhomogeneous materials were developed by Chalivendra and Shukla [28]. In their work, an effort has been made to ascertain the need for taking into account transient effects during crack growth. This motivated them to perform experiments using a different specimen geometry [59]. They performed mode-I dynamic fracture experiments in such a way that a highly transient elastodynamic crack-growth history could be generated. The phenomenon of transition from a stationary to a fully dynamic, rapidly propagating crack was studied.

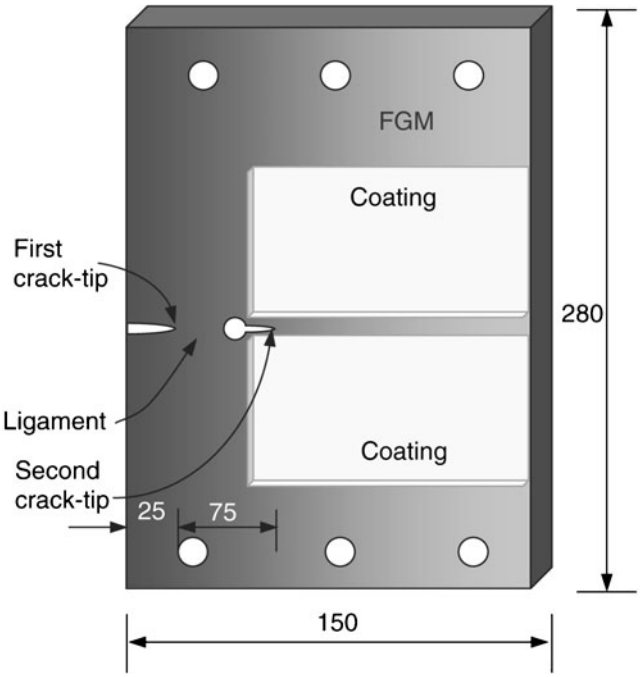

Fig. 18 FGM-SENT specimen [59]

A novel specimen geometry was designed as shown in Fig. 18. Two cracks were inserted with the first one located such that the subsequent crack propagation would be in an increasing fracture toughness direction. The specimen was loaded to a predetermined value K_Q (initial static SIF) and the crack was initiated from the first crack by drawing a sharp knife-edge across the tip. The crack propagated across the un-cracked ligament between the two crack tips before arresting temporarily at the second crack tip. Subsequently, the value of the

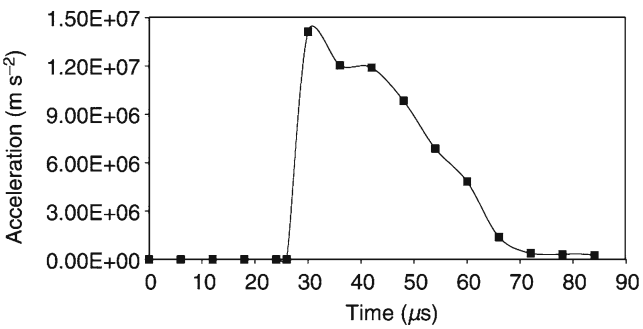

Fig. 19 Crack-tip acceleration as a function of time [59]

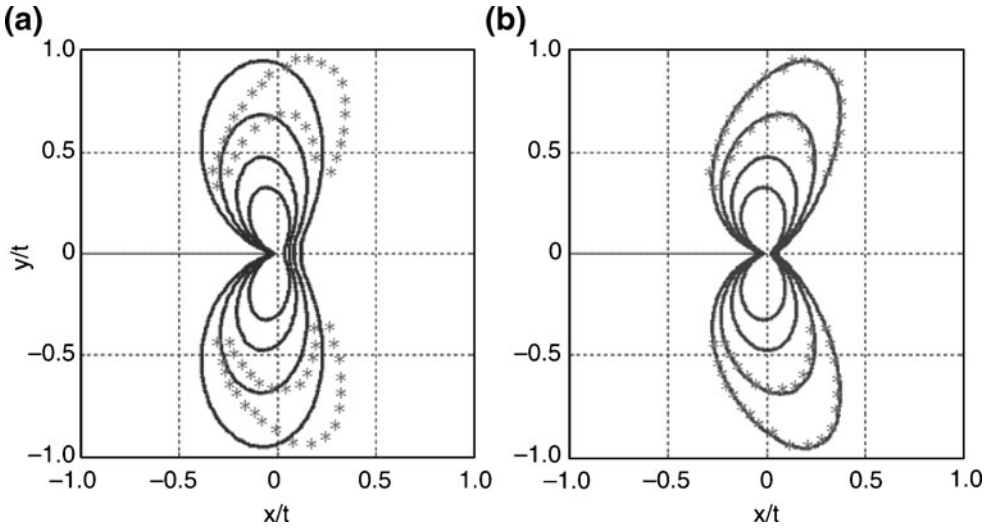

Fig. 20 Effect of transient higher-order terms on analysis of experimental data [59]

SIF increased steadily at the second crack tip until it became sufficiently large to produce re-initiation and resumption of crack growth. The bluntness of the second crack tip was controlled so that the crack stationary for a relatively long time (approximately 200 μs) and re-initiation occurred at relatively high values of K_Q. The transient nature of the event was demonstrating in terms of crack acceleration (with jumps of several orders of magnitude) followed by multiple oscillations, leading to eventual arrest (Fig. 19).

Analysis of fringes indicated that neglecting the transient higher-order terms could generate errors in SIF, as high as 20%. However, in regions where crack tip acceleration reduces substantially, the instantaneous SIF obtained using a transient analysis and a steady-state analysis was in good agreement. This was further illustrated by overlaying the analytical solution with and without transient effects on experimental data points (see, Fig. 20). Comparatively, exclusive use of a homogeneous solution results in 30% error in the analysis.

Summary and Future Prospects

In spite of the variety of materials and methods used to date in optical investigation of fracture behavior of FGMs, several common themes have emerged. Many of these works provide a fundamental understanding of the basic fracture behavior of the material. For instance, it has been shown, both theoretically and experimentally, that the asymptotic 2D displacement fields describing fracture retain the characteristics associated with homogeneous materials in the first two powers of r. However, for all higher powers of r, the influence of nonhomogeneity does exist. Consequently, the use of a K-dominant description of crack tip fields requires caution in certain types of FGMs. In particular, inclusion of the T-stress has been shown to be essential in reconciling theory and experimentation. Further, this deviation becomes more pronounced in situations when transient effects are significant.

Beyond the mechanical field characteristics, practical inferences can be readily drawn as well. For cases where the crack is oriented perpendicularly to the gradient direction, the stress field is inherently mixed-mode, even when the loading conditions is one of pure mode-I. In addition, the burden of material deformation is shouldered by the compliant regions of the specimen. Furthermore, the performance of the FGMs in this configuration is superior to that of bimaterials.

When the crack is in the direction of gradation, it has been demonstrated that under quasi-static conditions the FGM is capable of sustaining higher load with the crack located on the compliant side of the FGM than when it resides on the stiffer side. Under dynamic conditions, however, locating the crack on the compliant side of the material promotes faster and more effortless propagation than when the crack is on the stiffer side. Also, within the dynamic environment, several experiments have shown that the influences of the elastic modulus variation take precedence over local micro structure. The mixed-mode behavior of an FGM crack distinguishes itself by the eccentricity of its stress field and its propensity for kinking, particularly when the crack is in the direction of increasing gradation. In the limited number of experiments reported thus far, unlike the homogeneous counterparts, the results hint at the

possibility of crack growth in FGMs with a non-zero mode-II stress intensity factor. Further investigation is needed to fully resolve this question.

Other aspects of FGM fracture research that needs attention include (a) addressing the equivalence between materials within the FGM category itself, or between FGMs, on the one side, and homogeneous- or bi-materials, on the other side, (b) incorporating FGM architectures in structural configurations such as sandwich structures and demonstrating improvements in failure responses, and (c) conducting controlled experiments to study fracture behavior of FGMs under thermo-mechanical loading conditions.

Acknowledgements HVT would like to gratefully acknowledge the support of a grant from the U.S. Army Research Office (Grant No. W911NF-04-10257). CER acknowledges the support of the U.S. Army Research Office ARO Solid Mechanics Program (46449-EG) and from the University of Rhode Island DHS Center of Excellence in Explosives. AS wishes to acknowledge the financial support of the Air Force of Scientific Research under grant no. FA 95500910639 and the National Science Foundation under grant no. CMS 0244330.

References

1. Hirano T, Yamada T, Teraki J, Nino M, Kumakawa A (1988) A study on a functionally graded material design system for a thrust chamber. In: Proceedings 16th international symposium on space technology and science, Sapporo, Japan
2. Jin ZH, Batra RC (1996) Some basic fracture mechanics concepts in functionally graded materials. J Mech Phys Solids 44(8):1221–1235
3. Sasaki M, Hirai T (1991) Fabrication and properties of functionally gradient materials. Nippon Seramikkusu Kyōkai Gakujutsu Rombunsh—J Ceram Soc Jpn 99(10):1002–1013
4. Bishop A, Lin CY, Navaratnam M, Rawlings RD, Mcshane HB (1993) A functionally gradient material produced by a power metallurgical process. J Mater Sci Lett 12(19):1516–1518
5. Chu J, Ishibashi H, Hayashi K, Takebe H, Morinaga K (1993) Slip casting of continuous functionally gradient material. Nippon Seramikkusu Kyōkai Gakujutsu Rombunsh—J Ceram Soc Jpn 101(7):841–844
6. Sampath S, Gansert R, Herman H (1995) Plasma-spray forming ceramics and layered composites. J Miner Met Mater Soc 47(10):30–33
7. Parameswaran V, Shukla A (1998) Dynamic fracture of a functionally gradient material having discrete property variation. J Mater Sci 33(13):3303–3311
8. Butcher RJ, Rousseau CE, Tippur HV (1998) A functionally graded particulate composite: preparation, measurements and failure analysis. Acta Mater 47(1):259–268
9. Parameswaran V, Shukla A (2000) Processing and characterization of a model functionally gradient material. J Mater Sci 35(1):21–29
10. Atkinson C, List RD (1978) Steady-state crack-propagation into media with spatially varying elastic properties . Int J Eng Sci 16(10):717–730
11. Delale F, Erdogan F (1983) The crack problem for a nonhomogeneous plane. J Appl Mech Trans ASME 50(3):609–614
12. Williams ML (1957) On the stress distribution at the base of a stationary crack. J Appl Mech Trans ASME 24:109–114
13. Eischen JW (1987) Fracture of nonhomogeneous materials. Int J Fract 34(1):3–22
14. Eftis J, Subramonian N, Liebowitz H (1977) Crack border stress and displacement equations revisited. Eng Fract Mech 9(1):189–210
15. Parameswaran V, Shukla A (2002) Asymptotic stress fields for stationary cracks along the gradient in functionally graded materials. J Appl Mech Trans ASME 69(3):240–243
16. Chalivendra VB, Shukla A, Parameswaran V (2003) Quasistatic stress fields for a crack inclined to the property gradation in functionally graded materials. Acta Mech 162(1–4):167–184
17. Jain N, Rousseau CE, Shukla A (2004) Crack-tip stress fields in functionally graded materials with linearly varying properties. Theor Appl Fract Mech 42(2):155–170
18. Chalivendra VB (2008) Mode-I crack-tip stress fields for inhomogeneous orthotropic medium. Mech Mater 40(4–5):293–301
19. Chalivendra VB (2009) Mixed-mode crack-tip stress fields for orthotropic functionally graded materials. Acta Mech 204(1–2):51–60
20. Krenk S (1979) Elastic-constants of plane orthotropic elasticity. J Compos Mater 13:108–116
21. Westergaard HM (1939) Bearing pressures and cracks. J Appl Mech Trans ASME 6(5):A49–A53
22. Erdogan F, Wu BH (1997) The surface crack problem for a plate with functionally graded properties. J Appl Mech Trans ASME 64(3):449–456
23. Parameswaran V, Shukla A (1999) Crack-tip stress fields for dynamic fracture in functionally gradient materials. Mech Mater 31(9):579–596
24. Chalivendra VB, Shukla A, Parameswaran V (2002) Dynamic out of plane displacement fields for an inclined crack in graded materials. J Elast 69(1–3):99–119
25. Shukla A, Jain N (2004) Dynamic damage growth in particle reinforced graded materials. Int J Impact Eng 30(7):777–803
26. Lee KH (2004) Characteristics of a crack propagating along the gradient in functionally gradient materials. Int J Solids Struct 41(11–12):2879–2898
27. Jain N, Shukla A (2004) Displacements, strains and stresses associated with propagating cracks in materials with continuously varying properties. Acta Mech 171(1–2):75–103
28. Chalivendra VB, Shukla A (2005) Transient elastodynamic crack growth in functionally graded materials. J Appl Mech Trans ASME 72(2):237–248
29. Chalivendra VB (2007) Asymptotic analysis of transient curved crack in functionally graded materials. Int J Solids Struct 44(2):465–479
30. Lee KH, Chalivendra VB, Shukla A (2008) Dynamic crack-tip stress and displacement fields under thermomechanical loading in functionally graded materials. J Appl Mech Trans ASME 75(5):1–7
31. Erdogan F (1985) The crack problem for bonded nonhomogeneous materials under antiplane shear loading. J Appl Mech Trans ASME 52(4):823–828
32. Erdogan F, Kaya AC, Joseph PF (1991) The mode-III crack problem in bonded materials with a nonhomogeneous interfacial zone. J Appl Mech Trans ASME 58(2):419–427
33. Ozturk M, Erdogan F (1995) An axisymmetrical crack in bonded materials with a nonhomogeneous interfacial zone under torsion. J Appl Mech Trans ASME 62(1):116–125

34. Chan YS, Paulino GH, Fannjiang AC (2001) The crack problem for nonhomogeneous materials under antiplane shear loading—a displacement based formulation. Int J Solids Struct 38(17):2989–3005
35. Wang BL, Mai YW, Noda N (2004) Fracture mechanics analysis models for functionally graded materials with arbitrarily distributed properties (modes II and III problems). Int J Fract 126(4):307–320
36. Paulino GH, Fannjiang AC, Chan YS (2003) Gradient elasticity theory for mode III fracture in functionally graded materials—part I: crack perpendicular to the material gradation. J Appl Mech Trans ASME 70(4):531–542
37. Chan Y-S, Paulino GH, Fannjiang AC (2008) Gradient elasticity theory for mode III fracture in functionally graded materials—part II: crack parallel to the material gradation. J Appl Mech Trans ASME 75(6):061015-1–061015-11
38. Kubair DV, Geubelle PH, Lambros J (2005) Asymptotic analysis of a mode III stationary crack in a ductile functionally graded material. J Appl Mech Trans ASME 72(4):461–467
39. Tippur HV, Krishnaswamy S, Rosakis AJ (1991) Optical mapping of crack tip deformations using the methods of transmission and reflection coherent gradient sensing—a study of crack tip K-dominance. Int J Fract 52(2):91–117
40. Rousseau CE, Tippur HV (2000) Compositionally graded materials with cracks normal to the elastic gradient. Acta Mech 48(16):4021–4033
41. Gu P, Asaro RJ (1997) Crack deflection in functionally graded materials. Int J Solids Struct 34(24):3085–3098
42. Abanto-Bueno J, Lambros J (2006) An experimental study of mixed mode crack initiation and growth in functionally graded materials. Exp Mech 46(2):179–196
43. Lambros J, Santare MH, Li H, Sapna GH (1999) A novel technique for the fabrication of laboratory scale model functionally graded materials. Exp Mech 39(3):184–190
44. Peters WH, Ranson WF (1982) Digital imaging techniques in experimental stress-analysis. Opt Eng 21(3):427–431
45. Chu TC, Ranson WF, Sutton MA, Peters WH (1985) Applications of digital-image-correlation techniques to experimental mechanics. Exp Mech 25(3):232–244
46. Oral A, Lambros J, Anlas G (2008) Crack initiation in functionally graded materials under mixed mode loading: experiments and simulations. J Appl Mech Trans ASME 75(5):051110
47. Li H, Lambros J, Cheeseman BA, Santare MH (2000) Experimental investigation of the quasi-static fracture of functionally graded materials. Int J Solids Struct 37(27):3715–3732
48. Honein T, Herrmann G (1997) Conservation laws in nonhomogeneous plane elastostatics. J Mech Phys Solids 45(5):789–805
49. Rousseau CE, Tippur HV (2002) Evaluation of crack tip fields and stress intensity factors in functionally graded elastic materials: cracks parallel to elastic gradient. Int J Fract 114(1):87–111
50. Abanto-Bueno J, Lambros J (2002) Investigation of crack growth in functionally graded materials using digital image correlation. Eng Fract Mech 69(14-16):1695–1711
51. Abanto-Bueno J, Lambros J (2006) Parameters controlling fracture resistance in functionally graded materials under mode I loading. Int J Solids Struct 43(13):3920–3939
52. Rousseau C-E (2006) Critical examination of the use of coherent gradient sensing in measuring fracture parameters in functionally graded materials. J Compos Mater 40(19):1763–1782
53. Rousseau CE, Tippur HV (2001) Dynamic fracture of compositionally graded materials with cracks along the elastic gradient: experiments and analysis. Mech Mater 33(7):403–421
54. El-Hadek MA, Tippur HV (2003) Dynamic fracture parameters and constraint effects in functionally graded syntactic epoxy foams. Int J Solids Struct 40(8):1885–1906
55. Kirugulige MS, Kitey R, Tippur H (2005) Dynamic fracture behavior of model sandwich structures with functionally graded core: a feasibility study. Compos Sci Technol 65(7–8):1052–1068
56. Kirugulige MS, Tippur HV (2006) Mixed-mode dynamic crack growth in functionally graded glass-filled epoxy. Exp Mech 46(2):269–281
57. Kirugulige M, Tippur HV (2008) Mixed-mode dynamic crack growth in a functionally graded particulate composite: experimental measurements and finite element simulations. J Appl Mech—Trans ASME 75(5):051102.1–051102.14
58. Jain N, Shukla A (2006) Mixed mode dynamic fracture in particulate reinforced functionally graded materials. Exp Mech 46(2):137–154
59. Shukla A, Jain N, Chona R (2007) A review of dynamic fracture studies in functionally graded materials.Strain 43(2):76–95